Heliyon 10 (2024) e38871

Contents lists available at ScienceDirect

Heliyon

journal homepage: www.cell.com/heliyon

Research article

Investigation of Lysophospholipids-DHA transport across an *in vitro* human model of blood brain barrier

Maysa Hachem [a,*], Abdelmoneim H. Ali [b], Ibrahim Yildiz [c], Christophe Landry [d], Fabien Gosselet [d]

[a] *Department of Chemistry, College of Engineering and Physical Sciences, Khalifa University of Science and Technology, Abu Dhabi, 127788, United Arab Emirates*
[b] *Department of Chemical & Petroleum Engineering, College of Engineering and Physical Sciences, Khalifa University of Science and Technology, Abu Dhabi, 127788, United Arab Emirates*
[c] *Department of Chemistry, Khalifa University of Sciences and Technology, Abu Dhabi, 127788, United Arab Emirates*
[d] *Artois University, Blood-Brain Barrier Laboratory, UR 2465, Lens, France*

ARTICLE INFO

Keywords:
Brain lipids
Omega-3 fatty acids
Docosahexaenoic acid
Lysophospholipids
Fatty acid transport
Blood-brain-barrier
Recovery
LC-MS
Molecular modeling

ABSTRACT

Several studies emphasized on the preventive and therapeutic potential of Docosahexaenoic Acid (DHA, 22:6n-3) supplementation in chronic and age-related disorders including neurodegenerative diseases. Researchers principally studied the cerebral accretion of Lysophosphatidylcholine (LysoPC-DHA), the furthermost vital Lysophospholipid-DHA (LysoPL-DHA) in blood plasma. Nevertheless, the cerebral bioavailability of other LysoPL-DHA forms including Lysophosphatidylethanolamine (LysoPE-DHA), and Lysophosphatidylserine (LysoPS-DHA) were not extensively examined even though their vital biological functions in the brain. Hence, the aim of the present study was to evaluate the toxicity and transport of DHA in comparison to several LysoPL-DHA including LysoPC-DHA, LysoPE-DHA and LysoPS-DHA across a human model of blood-brain barrier (BBB). The human brain-like endothelial cells (hBLECs) monolayer tightness was evaluated by the parallel assessment of the permeability of fluorescent marker Lucifer yellow (LY) and revealed the absence of toxicity of non-esterified DHA and all LysoPL-DHA towards hBLECs. LysoPC-DHA, LysoPE-DHA and LysoPS-DHA displayed a higher recovery in the abluminal medium in comparison to non-esterified DHA at 30, 60 and 120 min post-incubation. Among all, LysoPS-DHA revealed the highest apparent coefficient permeability (Papp) 85.87 $\pm$ 4.24 x 10^{-6} cm s^{-1} and was significantly different than DHA, LysoPC-DHA and LysoPE-DHA. More interestingly, when studying the time course of Papp of DHA, LysoPC-DHA and LysoPE-DHA, at different post-incubation time, this permeability decreases with time especially for LysoPC-DHA and LysoPE-DHA, not for DHA. Furthermore, LysoPS-DHA exhibited the highest intracellular accumulation (10.39 $\pm$ 0.49 %) in hBLECs in comparison to all other tested lipids. Finally, differences in 3D structures and molecular electrostatic potential maps calculation of LysoPL-DHA could explain the dissimilar cerebral uptake of LysoPL-DHA. Altogether, our findings raise the novel hypothesis that LysoPS-DHA may represent a preferred physiological carrier of DHA to the brain.

* Corresponding author.
E-mail address: mayssa.hachem@ku.ac.ae (M. Hachem).

https://doi.org/10.1016/j.heliyon.2024.e38871
Received 10 May 2024; Received in revised form 27 September 2024; Accepted 1 October 2024
Available online 2 October 2024

1. Introduction

Neurodegenerative diseases including Alzheimer's (AD) and Parkinson's (PD) diseases are associated with high morbidity and mortality rates. Despite the fact that there is no treatment to cure these diseases, several drugs have been manufactured to slow down their progress [1,2].

For many decades, researchers have emphasized on the beneficial effects of omega-3 polyunsaturated fatty acids (PUFA), particularly docosahexaenoic acid (DHA, 22:6 n-3) in the brain [3–8], where DHA is the foremost PUFA essential for cerebral development and functions [9]. A decrease in the cerebral quantity of DHA was identified in patients suffering from neurodegenerative diseases, such as AD and PD [10]. Along with exogenous supply of DHA through marine sources (fish oils, microalgae, etc.), DHA can be endogenously synthesized *via* elongation and desaturation of eicosapentaenoic acid (EPA, 20:5 n-3) or through the elongation of its precursor α-linolenic acid (ALA, 18:3 n-3) [11,12]. However, the conversion of ALA into DHA through elongation process is very low in human. Thus, targeted intake of DHA to the brain might compensate its deficiency in AD and PD patients [13].

Therefore, scientists have explored this research topic and investigated the brain' supply with DHA in different forms, whether non-esterified DHA or esterified in different lipid species. The main challenge remains the passage of these molecules across the blood-brain-barrier (BBB), which is a physical and metabolic barrier preserving the cerebral homeostasis [3,14–20]. BBB is composed by the brain endothelial cells lining the cerebral blood vessels and surrounded by brain pericytes that are embedded in the same basal lamina.

Among researchers, Thies et al. examined whether unsaturated 2-acyl-lysophosphatidylcholine (2-acyl-LysoPC) bound to plasma albumin was a privileged carrier of unsaturated fatty acids (FAs) to 20-days-old rats' brain in comparison to non-esterified forms of these FAs [21]. Labeled ^{14}C palmitic, ^{14}C oleic, ^{14}C linoleic, and ^{14}C arachidonic acids in either their non-esterified form or esterified in LysoPC labeled with ^{3}H on the choline and ^{14}C FAs moieties were perfused for 30 s. Results showed that 2-acyl-LysoPC was an efficient delivery form of unsaturated FAs to the rat brain, and FAs delivery form could control their fate in tissues. The same team investigated the uptake and metabolism of ^{3}H-DHA esterified at *sn*-2 position of LysoPC-DHA (^{3}H-LysoPC-DHA) and in non-esterified form in 20-days-old rats through perfusion of 100 μL of lipids solution with 1 μCi of LysoPC with ^{3}H-DHA (12 nmols) into the tail vein for 30 s. They reported that ^{3}H-LysoPC-DHA was preferentially recovered in the brain (4–5% of injected radioactivity) over the non-esterified form of DHA (0.3–0.4 %) [18]. Later, within the same research field, Bernoud et al. conducted an *in vitro* study for cerebral accretion of DHA esterified at *sn*-2 position of ^{3}H-LysoPC-DHA as compared to non-esterified form of ^{3}H-DHA. ^{3}H-LysoPC-DHA was a favored functional carrier of DHA to the brain when compared to non-esterified ^{3}H-DHA [19]. More recently, Hachem et al. evaluated *in vitro*, *in vivo*, and *ex-vivo* the cerebral accretion of a structured phosphatidylcholine named 1-acetyl,2-docosahexaenoyl-glycerophosphocholine (AceDoPC®) in comparison to other DHA forms. AceDoPC® is considered a stabilized physiological LysoPC-DHA form with an acetyl moiety at *sn-1* position instead of hydroxyl moiety in LysoPC-DHA [14,15,22–24]. By combining *in vitro* and *in vivo* experiments, Hachem et al., revealed that AceDoPC® was a privileged and specific carrier of DHA to the brain, not in other organs, when compared with DHA containing PC and non-esterified DHA forms [25]. AceDoPC® was partially hydrolyzed into LysoPC-DHA [25]. Moreover, *ex-vivo*, Hachem et al. investigated the bioavailability of ^{13}C-DHA in elderly (60–70 years old) after an oral intake of a single dose (50 mg) of ^{13}C-DHA whether non-esterified or esterified in ^{13}C-AceDoPC® or esterified in triacylglycerols (^{13}C-TAG) [15]. Gas chromatography/Combustion/Isotope Ratio Mass Spectrometry (GC/C/IRMS) assessed ^{13}C enrichment of DHA-containing lipids. DHA from AceDoPC® was more efficient than from TAG for a sustained accumulation in the red cell ethanolamine phospholipids (PL), which had been associated with increased brain accretion [15].

As previously discussed, researchers mainly studied the cerebral accretion of LysoPC-DHA, the most abundant LysoPL-DHA in blood plasma [26]. However, the cerebral bioavailability of other LysoPL-DHA forms, such as Lysophosphatidylethanolamine (LysoPE), and Lysophosphatidylserine (LysoPS) are not widely explored despite their biological functions in the brain. Indeed, LysoPE-DHA is the second highest LysoPL in human plasma after LysoPC with 10–50 μM. In brain, LysoPE-DHA was reported to be implicated in the stimulation of neurite's growth and could be a hippocampal indicator of post-ischemic cognitive impairment [16]. Furthermore, Major Facilitator Superfamily Domain-containing protein 2 (Mfsd2a), known as LysoPC-DHA's receptor, is also a receptor for LysoPE to mediate DHA in the brain. However, the transfer of LysoPE-DHA across the BBB is still ambiguous and needs further investigation. Regarding LysoPS-DHA, it is also detected in human plasma, yet at significantly lower concentrations $<$0.1 μM. In brain, LysoPS-DHA transfer remains unclear despite its anti-inflammatory potential in neurodegenerative diseases [26].

Moreover, within the same thematic, previous researches tested the biomolecules *via* animal models of *in vitro* BBB whereas strong data with human preclinical models is required instead of using animal models mainly due to inter-species differences existing between human and animal BBB [27].

Hence, our research project aimed first to produce several LysoPL-DHA including LysoPC-DHA, LysoPE-DHA and LysoPS-DHA since these lipids are not commercially available. All LysoPL-DHA were produced through enzymatic hydrolysis of fatty acid at *sn-1* position, purified and quantified through optimization of several analytical techniques mainly Liquid Chromatography-Mass Spectrometry (LC-MS). Following, we investigated their cerebral bioavailability using an *in vitro* model of the human BBB in order to identify the privileged carrier of DHA to the central nervous system. This BBB model consists of co-cultivating hematopoietic stem cells with human brain pericytes. In few days, the endothelial cells acquire several *in vivo* features and are consequently named human brain-like endothelial cells (hBLECs). This model is used to assess toxicity of molecules and to predict brain distribution of drugs [28–30]. We measured the toxicity of DHA and LysoPL-DHA and investigated the permeabilities of non-esterified DHA, LysoPC-DHA, LysoPE-DHA and LysoPS-DHA across hBLECs. Furthermore, in order to better understand the effect of physical characteristics on the uptake and metabolism of these molecules in the brain, we examined the 3D structures, molecular electrostatic potential (ESP) maps and lipophilic potentials at the surfaces of the synthesized LysoPL-DHA.

Overall, our study focusing on the production of DHA-rich LysoPLs and investigation of their passage across the human model of BBB could pave the way for pharmaceutical applications since the actual commercially available DHA supplements are in the form of PLs or TGs which are not the preferred transporters of DHA to the brain based on all researches conducted until this day. The identification of the privileged carrier of LysoPL-DHA among the three studied here, will guide us to explore the potential therapeutic targeting brain diseases mainly through future *in vivo* and clinical studies.

2. Materials and methods

2.1. Chemicals and reagents

In our experiments, all chemicals and reagents were of analytical grade and high purity. Detailed information about the chemicals used in experiments were highlighted in Table 1. Organic solvents, including chloroform, ethanol, diethyl ether, methanol and isopropanol LC-MC grade were purchased from CHROMASLV®Riedel-de Haën Honeywell, USA. Ammonium formate eluent additive for LC-MS was bought from LiChropur TM ≥ 99.0 % Sigma-Aldrich, St. Louis, MO, USA. Lucifer Yellow (LY), Boric acid, calcium chloride, and phosphate buffer were purchased from Sigma Aldrich, Darmstadt, Germany.

In addition, Docosahexaenoic acid≥ 98 %, 1-palmitoyl,2-docosahexaenoyl-*sn*-glycero-3-phosphatidylcholine, 1-palmitoyl,2-docosahexaenoyl-*sn*-glycero-3-phosphoethanolamine, and 1-palmitoyl, 2-docosahexaenoyl-*sn*-glycero-3-phospho-L-serine were purchased from Sigma-Aldrich, St. Louis, MO, USA. 1-oleoyl-2-hydroxy-*sn*-glycero-3-phosphocholine, 1-oleoyl-2-hydroxy-*sn*-glycero-3-phosphoethanolamine, 1-oleoyl-2-hydroxy-*sn*-glycero-3-phospho-L-serine (sodium salt) were procured from Avanti polar lipids, Inc., USA. Amano lipase M from *Mucor javanicus* (≥10,000 U/g) was purchased from Sigma Aldrich. PK30 Supelclean LC-Si (Sep-Pak) 1G/6 ML were acquired from Supelco by Sigma-Aldrich, St. Louis, USA.

2.2. Production and purification of LysoPL-DHA

LysoPC-DHA, LysoPE-DHA, and LysoPS-DHA were produced *via* the enzymatic hydrolysis of *sn-1* position of commercial PL-DHA (PC-DHA, PE-DHA, PS-DHA) purchased from Sigma-Aldrich as mentioned in section "Chemicals and reagents".

Briefly, 10 mg of Amano lipase M enzyme were mixed with 1 mL phosphate buffer (20 mM, pH 7.2). Then, 1.2 μmoles of PL-DHA (whether) were dissolved in 100 μL of methanol CH_3OH. PL-DHA solutions were added to the enzyme solution, and the mixtures were agitated for 3 h at 800 rpm and 40 °C following the method reported by Devos et al. [31]. Indeed, Devos et al., 2006 hydrolyzed the

Table 1
List of chemicals used in analysis and extraction.

Chemical	CAS number	Catalogue number	Company name	Address
Chloroform	67-66-3	650471	CHROMASLV®Riedel-de Haën Honeywell	USA
Ethanol	64-17-5	34852	CHROMASLV®Riedel-de Haën Honeywell	USA
Diethyl ether	60-29-7	I0069	CHROMASLV®Riedel-de Haën Honeywell	USA
Methanol LC-MS	34966	14262	CHROMASLV®Riedel-de Haën Honeywell	USA
Isopropanol LC-MS	67-63-0	34965	CHROMASLV®Riedel-de Haën Honeywell	USA
Ammonium formate	540-69-2	17843	LiChropur, Sigma-Aldrich	St. Louis, MO, USA
Lucifer Yellow	77944-88-8	71206-95-6	Sigma Aldrich	Darmstadt, Germany
Boric acid	10043-35-3	B6768	Sigma Aldrich	Darmstadt, Germany
Calcium chloride	10043-52-4	102378	Sigma Aldrich	Darmstadt, Germany
Phosphate buffer	7778-77-0	146777	Sigma Aldrich	Darmstadt, Germany
Docosahexaenoic acid	6217-54-5	D2534	Sigma-Aldrich	St. Louis, MO, USA
1-palmitoyl,2-docosahexaenoyl-*sn*-glycero-3-phosphatidylcholine	59403-54-2	850461C	Sigma-Aldrich	St. Louis, MO, USA
1-palmitoyl,2-docosahexaenoyl-*sn*-glycero-3-phosphoethanolamine	96998-00-4	850801C	Sigma-Aldrich	St. Louis, MO, USA
1-palmitoyl, 2-docosahexaenoyl-*sn*-glycero-3-phospho-L-serine	474943-17-4	840062C	Sigma-Aldrich	St. Louis, MO, USA
1-oleoyl-2-hydroxy-*sn*-glycero-3-phosphocholine	19420-56-5	845875P	Avanti polar lipids	Alabaster, AL, USA
1-oleoyl-2-hydroxy-*sn*-glycero-3-phosphoethanolamine	89576-29-4	846725P	Avanti polar lipids	Alabaster, AL, USA
1-oleoyl-2-hydroxy-*sn*-glycero-3-phospho-L-serine	326589-90-6	858143P	Avanti polar lipids	Alabaster, AL, USA
Amano lipase M from *Mucor javanicus*	9001-62-1	5348803	Sigma Aldrich	St. Louis, MO, USA

total phospholipids extracted from microalgal biomass using the enzymatic preparation mentioned above and not specifically for the production of LysoPC-DHA, LysoPE-DHA and LysoPS-DHA. Hence, when we tested this enzymatic reactions on commercial PC-DHA, PE-DHA and PS-DHA, we could produce the targeted molecules.

For lipids extraction, 1 mL of CH_3OH and 2 mL of chloroform $CHCl_3$ were added to the mixture which was centrifuged for 10 min at 4000 rpm, 4 °C. The $CHCl_3$ fraction was recovered and the same process was repeated twice. The extracted lipids were recovered in 1 mL of $CHCl_3/CH_3OH$ (2:1, v/v).

The hydrolysis of PL-DHAs was followed during and at the end of the reaction through thin layer chromatography TLC analysis. LysoPL-DHAs produced were collected and purified through Solid Phase Extraction (SPE) technique with a normal gradient Sep-Pak column and a gradient of solvents consisting of $CHCl_3$, $CHCl_3/CH_3OH$ (90:10, v/v), $CHCl_3/CH_3OH$ (80:20, v/v), $CHCl_3/CH_3OH$ (70:30, v/v), $CHCl_3/CH_3OH$ (60:40, v/v), $CHCl_3/CH_3OH$ (50:50, v/v), and CH_3OH. Pure LysoPL-DHA fractions were eluted with $CHCl_3/CH_3OH$ (50:50, v/v), and CH_3OH. Solvents were evaporated and pure LysoPL-DHA fractions were suspended in 1 mL of CH_3OH for further analysis and quantification through Liquid Chromatography Mass Spectrometry (LC-MS).

The chemical structures of the synthesized LysoPL-DHA of interest are illustrated in Fig. 1.

2.3. Liquid Chromatography Mass Spectrometry (LC-MS) analysis

We developed a novel LC-MS approach in order to identify the purity and quantify the produced LysoPC-DHA, LysoPE-DHA and LysoPS-DHA as well as commercial non-esterified DHA before conducting the *in vitro* study. Since such data are not accessible in any database, we tested several protocols in house and selected the actual one described below which can be applied for future analysis and quantification of these molecules. The same LC-MS methodology was followed for analysis of lipids after testing their passage across the *in vitro* model of BBB.

For LC analysis, UPLC Shimadzu system (LCMS-8045, Kyoto, Japan) equipped with C18 analytical column (4.5 × 250 mm, 1.5 μm) was used. The flow rate was 500 μL/min and the column temperature was set at 50 °C. The sample chamber temperature was adjusted at 5 °C, and the injection volume was 5.0 μL for each analysis. The mobile phase consisted of two solvents: solvent A comprised isopropanol/methanol/water (5/1/4, v/v/v) while isopropanol was used as solvent B. 5 mM of ammonium formate was added to both solvents as an electrolyte. Acidic additives such as 0.2 % formic acid, which occasionally increase sensitivity in ESI-MS detection of the negative ion mode caused serious peak tailing in LC and was not applied in our analysis.

The effective separation of lipids was achieved with a binary gradient starting with 30 % B for 3 min, followed by a linear gradient to 80 % B from 3 to 7 min. Subsequently, the mobile phase was immediately returned to the initial conditions and maintained for 3 min until the end. The running time for each sample was 17 min.

For MS analysis, a triple quadruple mass spectrometer instrument (LCMS-8045, Kyoto, Japan) with electrospray ionization (ESI) probe was used for the identification and quantification of lipids.

Nebulizer gas (nitrogen) was used at a flow rate of 3.0 L/min, drying gas (nitrogen) at a flow rate of 6.0 L/min and argon as the collision gas. The probe temperature was set at 350 °C, and the desolvation line temperature was set at 100 °C.

Positive and negative ionization modes were applied at multiple-reaction monitoring (MRM) optimized conditions for analysis of standards as well as produced molecules (Table 2).

DHA, LysoPE-DHA, LysoPE-18:1, LysoPS-DHA and LysoPS-18:1 were analyzed in positive mode whereas LysoPC-DHA and LysoPC-

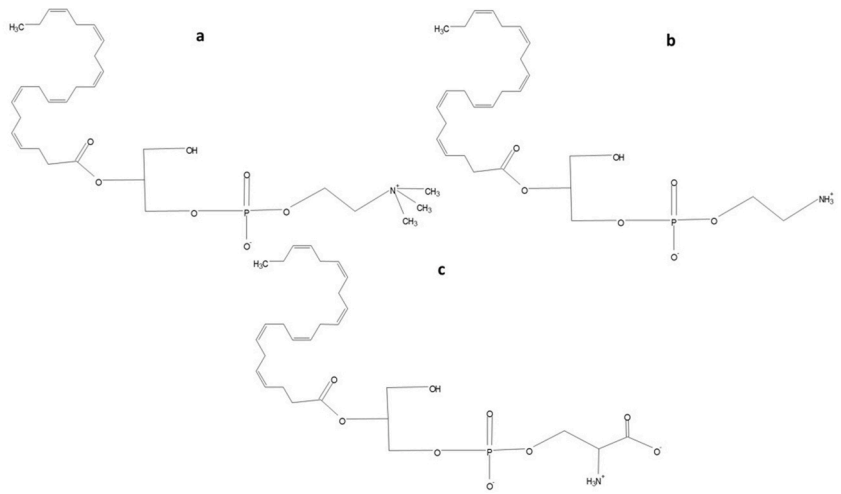

Fig. 1. Chemical structures of LysoPL with DHA esterified at *sn-2* position.
(a) 1-lyso,2-docosahexaenoyl-glycerophosphatidylcholine LysoPC-DHA; **(b)** 1-lyso,2-docosahexaenoyl-glycerophosphatidylethanolamine LysoPE-DHA; **(c)** 1-lyso, 2-docosahexaenoyl- glycerophosphatidylserine LysoPS-DHA. All chemical structures were created using Mestrelab Research Software Bruker.

Table 2
Optimized MRM conditions for the separation of the different lipid forms.

Compound	Precursor (*m/z*)	Product (*m/z*)	Pause Time (msec)	Dwell Time (msec)	Q1 Pre Bias	CE (volts)	Q3 Pre Bias
DHA	327.48	283.20	3.0	100.0	13.0	11.0	19.0
	327.48	281.25	3.0	100.0	13.0	7.0	12.0
	327.48	229.20	3.0	100.0	12.0	13.0	14.0
LysoPC-DHA	568.20	184.10	3.0	100.0	−28.0	−29.0	−20.0
	568.20	104.20	3.0	100.0	−28.0	−28.0	−11.0
	568.20	115.00	3.0	100.0	−28.0	−52.0	−24.0
LysoPC-18:1	522.67	184.10	3.0	100.0	−26.0	−26.0	−20.0
	522.67	104.15	3.0	100.0	−26.0	−25.0	−20.0
	522.67	125.10	3.0	100.0	−26.0	−50.0	23.0
LysoPE-DHA	525.30	328.20	3.0	100.0	20.0	20.0	21.0
	525.30	284.20	3.0	100.0	20.0	22.0	18.0
	525.30	196.00	3.0	100.0	20.0	28.0	19.0
LysoPE-18:1	478.58	281.30	3.0	100.0	13.0	25.0	18.0
	478.58	196.10	3.0	100.0	13.0	25.0	12.0
	478.58	79.00	3.0	100.0	13.0	48.0	24.0
LysoPS-DHA	569.20	364.85	3.0	100.0	26.0	16.0	16.0
	569.20	297.00	3.0	100.0	28.0	18.0	20.0
	569.20	228.90	3.0	100.0	28.0	23.0	14.0
LysoPS-18:1	544.57	153.10	3.0	100.0	26.0	34.0	29.0
	544.57	408.95	3.0	100.0	28.0	10.0	21.0
	544.57	341.05	3.0	100.0	28.0	16.0	15.0

18:1 in negative mode.

For quantification purposes, a mixture of standards DHA, LysoPC-18:1, LysoPE-18:1, LysoPS-18:1 was prepared. The concentration of each standard was 20 μM. DHA was quantified by using an external calibration curve while LysoPL-DHA were quantified by using LysoPC-18:1, LysoPE-18:1, and LysoPS-18:1 as internal standards respectively for LysoPC-DHA, LysoPE-DHA, and LysoPS-DHA. LabSolutions software (Ver. 5.86) was used for the analysis and interpretation of data.

2.4. In vitro model of human blood brain barrier

Human brain pericytes (HBPs) were provided by Dr. Fumitaka Shimizu and Takashi Kanda from department of Neurology and Clinical Neuroscience, Graduate School of Medicine, Yamaguchi University, Ube, Japan. HBPs were isolated from a patient who had suddenly died from a heart attack [32]. Study protocol for human tissue was approved by the ethics committee of the Medical Faculty (IRB#: H18-033-6), University of Yamaguchi Graduate School, and was conducted in accordance with the Declaration of Helsinki, as amended in Somerset West in 1996. For the $CD34^{+}$-hematopoietic stem cells, written informed consent was obtained from the family of the participant before entering the study. The collection of human umbilical cord blood requires infants' parents signed consent form in compliance with French legislation. The protocol was approved by the French Ministry of Higher Education and Research

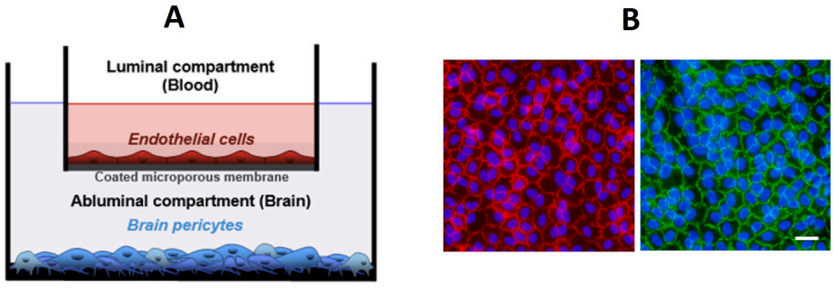

Fig. 2. *In vitro* model of human BBB. The model consists of a co-culture of human brain-like endothelial cells (hBLECs) with human brain pericytes (HBPs). Human brain pericytes (HBPs) were provided by Dr. Fumitaka Shimizu and Takashi Kanda from department of Neurology and Clinical Neuroscience, Graduate School of Medicine, Yamaguchi University, Ube, Japan. HBPs were isolated from a patient who had suddenly died from a heart attack. Study protocol for human tissue was approved by the ethics committee of the Medical Faculty (IRB#: H18-033-6), University of Yamaguchi Graduate School, and was conducted in accordance with the Declaration of Helsinki, as amended in Somerset West in 1996. According to the French legislation, the human cells were handled at the Blood-Brain Barrier laboratory, UR 2465, Artois University, Lens, France, under the agreement number L2-1235.
(A) The CD34+-endothelial derived cells are seeded on a coated-insert and co-cultivated during 6 days with human brain pericytes (HBPs). **(B)** Endothelial cells then acquire blood-brain barrier (BBB) phenotype and are then named human brain-like endothelial cells (hBLECs) [28,29,35]. In particular, they express the tight junctions proteins CLAUDIN-5 and ZO-1 at the cell border, restricting the passage of molecules across hBLEC monolayer. CLAUDIN-5 is labeled in Red, ZO-1 in Green, and nuclei are in blue. Bar = 20 μm. (For interpretation of the references to color in this figure legend, the reader is referred to the Web version of this article.)

(CODECOH Number DC2011-1321). All experiments were carried out in accordance with the approved protocol. HBPs and CD34+-hematopoietic stem cells were regularly checked for mycoplasma contamination, and Short Tandem Repeats (STR) analysis confirmed the absence of cross-contamination. According to the French legislation, the human cells were handled in the laboratory under the agreement number L2-1235.

One week after thawing, HBPs were trypsinized and 5×10^4 cells were seeded into each well of 12-well plates (Costar), 2 days before co-culture with human CD34+-derived endothelial cells (ECs). $CD34^+$ human stem cells were isolated from human umbilical cord blood and differentiated into the endothelial cells (ECs) according to the procedure reported by Pedroso, Tellechea [33]. Briefly, the isolated $CD34^+$ cells were cultured in EC growth medium MV 2 (PromoCell) and 50 ng/mL of vascular endothelial growth factor (VEGF, PrepoTech Inc), on 1 % gelatin-coated 24-well plates (2×10^5 cells/well). After 15–20 days, the ECs were seeded in the culture dish. The cells were expanded in 1 % (w/v) gelatin-coated T75 flasks (BD Biosciences) in EGM-2 medium and then frozen.

Polyethylene terephthalate (PET) filter inserts from Sarstedt with 1 μm filter pore size and a surface of 1.13 cm^2 (*i.e* 12-well inserts) were used (Ref #83.3931.101, Sarstedt, Germany). The upper side was coated with 1/48e diluted Matrigel (BD Biosciences, Le pont de claix, France).

In vitro BBB system was established by culturing the ECs on the upper side of the PET filter insert and pericytes in the well (Fig. 2). Frozen $CD34^+$-derived ECs were sub-cultured on gelatin-coated Petri dishes (Corning) in ECs growth medium MV 2 (Promocell) until confluence. Then, the ECs were trypsinized and seeded at a density of 8×10^4 cells per insert and the inserts transferred in 12-well plates in which HBPs were seeded 2 days before. The resulting co-culture was maintained for at least 6 days under standard conditions (37 °C in a humidified 5 % CO_2 atmosphere with renewal of the medium every 2 days). Under these conditions, the ECs obtained from $CD34^+$ human stem cells exhibited most of BBB characteristics, such as the low permeability to non-permeant markers, and therefore can be considered as a human *in vitro* BBB [34]. These cells are then named human Brain-like endothelial cells (hBLECs) [28,29,35].

2.5. Toxicity assessment of DHA and LysoPL-DHA

For toxicity studies, different concentrations of DHA, LysoPC-DHA, and LysoPE-DHA (1 and 10 μM) were evaluated. LysoPS-DHA was tested at one concentration only (1 μM) due to lack of product. We also tested Dimethyl Sulfoxide DMSO 1 % as positive controls of toxicity.

Lucifer Yellow (LY, 25 μM) was used as a paracellular marker to monitor the BBB permeability and assessing the toxicity of tested molecules. Indeed, this small hydrophilic molecule presents a low cerebral penetration and its endothelial permeability coefficient (Pe to LY) reveals the tightness of the endothelial cell monolayer.

Ringer–HEPES (RH buffer) buffer (150 mM NaCl, 5.2 mM KCl, 2.2 mM $CaCl_2$, 0.2 mM $MgCl_2$, $6H_2O$, 6 mM $NaHCO_3$, 5 mM HEPES, pH: 7.4) at 37 °C was added to empty wells in a 12-well plate (Costar). Filter inserts containing hBLECs were subsequently transferred in the 12-well plate and filled with RH containing the fluorescent integrity marker Sodium Fluorescein (LY; 10 μM; Sigma), which poorly crosses the BBB. Abluminal medium were retrieved at 30, 60, 120, and 180 min after incubation, whereas the luminal medium and hBLEC lysates were collected at 180 min. Analysis of LY fluorescence was performed using a fluorescence counter (Synergy H1, Biotek) using an excitation wavelength (λ) of 490 nm, and emission wavelength of 525 nm, and was determined in representative samples from each compartment of the triplicates and from the initial solution-containing drug in addition to LY.

The permeability coefficient was then calculated as previously described [36]. Briefly, both insert permeability (PSf, for insert only coated with Matrigel™) and permeability of inserts containing hBLECs (PSt, for insert with Matrigel™ and cells) were considered, according to the following formula: $1/PSe = 1/PSt - 1/PSf$. The permeability value for the hBLEC monolayer was then divided by the surface area of the insert (1.12 cm^2) to obtain the permeability coefficient (Pe) of each molecule (cm/min).

After completion of *in vitro* experiments, results regarding permeability to LY obtained in presence and absence of the test compounds were compared to ensure the integrity of endothelial cells monolayer during the transport experiment in presence of compound.

2.6. Endothelial apparent permeability and intracellular accumulation

DHA and LysoPL-DHA were incubated for 180 min at different concentrations (1 and 10 μM) on the luminal compartment of the human BBB model. DHA and LysoPL-DHA were added in 500 μL of RH buffer in the apical compartment of the insert of the BBB model. The insert is then placed on a 12-well plate filled with 1.5 mL of RH buffer. At 30, 60, 120 and 180 min, the inserts are placed in a new RH-filled well. At the end of the experiments, samples were taken from each compartment and lipids were quantified by LC-MS as described previously. Total lipids of luminal and abluminal medium were extracted according to the method of Bligh and Dyer [37] whereas total lipids of hBLECs were extracted by the method of Folch et al. [38]. The passage of the four different forms of DHA at 30, 60, 120, and 180 min across the *in vitro* human BBB model was assessed using LC-MS. The passage percentage of each compound across the BBB was calculated using the following equation:

$$\%\ \text{of initial concentration} = \frac{\text{Concentration of compound detected in compartment (Tmin)}}{\text{Concentration of compound in initial solution (T0 min)}} \times 100 \quad \text{(Eq.1)}$$

Additionally, the percentage of lipids passage across the model per minute was evaluated by dividing the quantity of lipids (DHA or LysoPL-DHA) that cross the BBB by the initial quantity added in the luminal compartment of the model and then divided by the time

factor.

Furthermore, endothelial apparent coefficient (Papp) of DHA and LysoPL-DHA were calculated as previously described by Santa-Maria AR et al., 2022 [39].

P_{app}, in $cm.s^{-1}$ determinates the rate of appearance or flux (J, in $amount.s^{-1}$) of the compound in the receiver compartment, thereby, normalizing for membrane surface area (S, in cm^2) and initial donor concentration at t_0 (C_0, in $amount.mL^{-1}$) (Eq. (2)).

$$Papp\ (\mathrm{cm}.s^{-1}) = \frac{J\ (amount.s^{-1})}{S\ (cm^2).C_0\left(amount.mL^{-1}\right)} \quad \text{Eq. 2}$$

Intracellular accumulation at 180 min have also been calculated and presented.

2.7. Immunofluorescence labelling

hBLECs were fixed with ice-cold methanol (20 s) for CLAUDIN-5 labelling or cold PFA 4 % (10 min) for ZO-1, and rinsed twice with cold PBS calcium and magnesium free (PBS-CMF; 8 g/L NaCl, 0.2 g/L KCl, 0.2 g/L KH_2PO_4, 2.86 g/L $Na_2HPO_4{\cdot}12H_2O$; pH 7.4). A step of 10 min-permeabilization (10 min at room temperature (RT)) with Triton X-100 0.1 % in PBS-CMF is required for PFA-fixed samples. Unspecific binding was blocked (30 min, RT) using a Sea Block buffer solution (SBBS, Thermo Fisher Scientific). Then, hBLECs were incubated (60 min, RT) with the primary antibodies against CLAUDIN-5 (1/100, Invitrogen, 34–1600) and ZO-1 (1/200, Invitrogen, 61–7300) in PBS-CMF containing 5 % (v/v) SBBS (PBS-SBBS). After rinsing, cells were incubated (30 min, RT) with a secondary polyclonal antibody (Life Technologies, A-11034) and 10 ng/mL DAPI (Invitrogen, D1306) for nuclear staining in PBS-SBBS. After rising, cells were mounted using ProLong Gold antifade mountant (Thermo Fisher). Images were acquired using a Leica microscope (DMi8; Leica Microsystems) and processed using the ImageJ software.

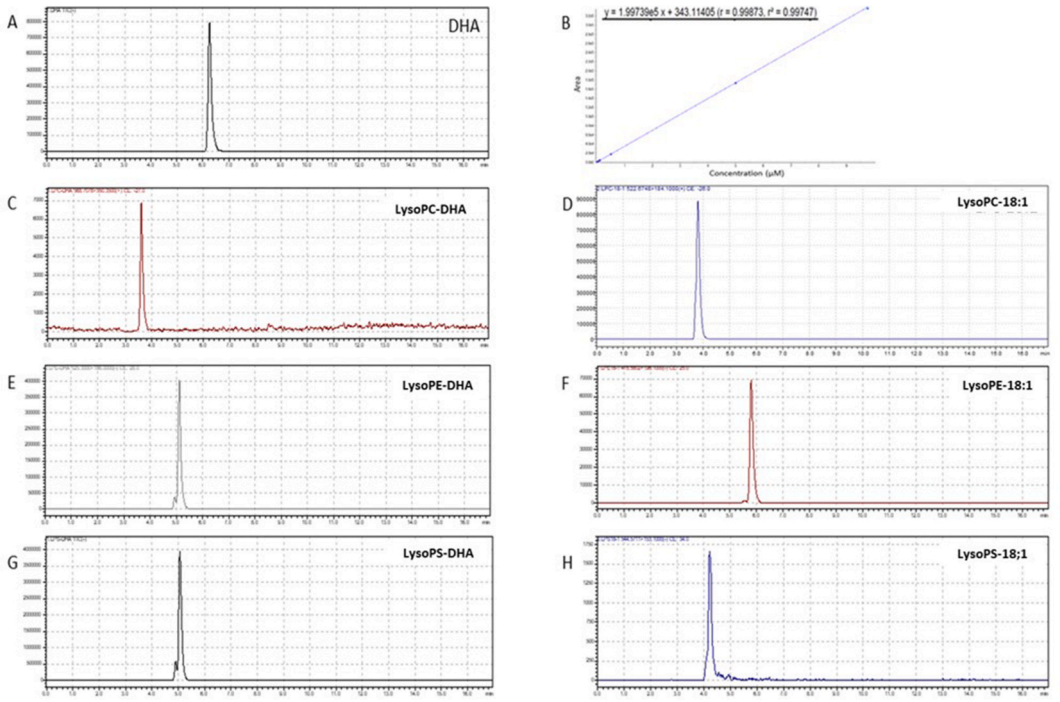

Fig. 3. Liquid Chromatography-Mass Spectroscopy (LC-MS) analysis of lipids. All lipids' analysis were conducted on an UPLC Shimadzu system (LCMS-8045, Kyoto, Japan) with C18 analytical column (4.5 × 250 mm, 1.5 µm), a flow rate of 500 µL/min and a column temperature of 50 °C. The sample chamber temperature was adjusted at 5 °C, and the injection volume was 5.0 µL for each analysis. The mobile phase consisted of solvent A comprised of isopropanol/methanol/water (5/1/4, v/v/v) while isopropanol was used as solvent B. 5 mM of ammonium formate was added to both solvents as an electrolyte. A binary gradient starting with 30 % B for 3 min, followed by a linear gradient to 80 % B from 3 to 7 min was applied for efficient separation of lipids. Afterward, the mobile phase was returned to the initial conditions and maintained for 3 min until the end. The total running time for each sample was 17 min. For MS analysis, a triple quadruple mass spectrometer instrument (LCMS-8045, Kyoto, Japan) with electrospray ionization (ESI) probe was used with a nebulizer gas (nitrogen) at a flow rate of 3.0 L/min, drying gas (nitrogen) at a flow rate of 6.0 L/min and argon as the collision gas. The probe temperature was 350 °C, and the desolvation line temperature was 100 °C. Positive and negative ionization modes were applied at multiple-reaction monitoring (MRM) optimized conditions for analysis of standards as well as produced molecules. **(A)** Total ion chromatogram of DHA; **(B)** Standard calibration curve of DHA (0–10 µM); Representative chromatograms of LysoPC-DHA **(C)**, LysoPC-18:1 **(D)**, LysoPE-DHA **(E)**, LysoPE-18:1 **(F)**, LysoPS-DHA **(G)**, and LysoPS-18:1 **(H)**.

2.8. Molecular modeling of LysoPL-DHA

In the body, it is well recognized that the physiological position of DHA in LysoPLs is the *sn-2* position whereas isomerization (passage of DHA from *sn-2* to *sn-1* position) can occur.

Although we have produced different *sn-2* LysoPL-DHA through enzymatic reaction, we compared the molecular modelling of both *sn-2* and *sn-1* LysoPL-DHA in order to verify similarities and differences which might be linked to the DHA position.

After energy minimization and evaluation with Gaussian 09 software, one model of LysoPC-DHA, LysoPE-DHA and LysoPS-DHA could be selected and considered as representative of the 3-D structure of these Lysophospholipids.

We considered the Density functional theory (DFT) calculations which was performed to optimize the geometries of the synthesized LysoPL-DHA by using M06-2X [40] DFT functional with Gaussian 09 package [41]. M06-2X functional was selected due to its better performance in the main-group chemistry [42]. In addition, minimum energy geometries were validated with the frequency calculations requiring no imaginary eigenvalues. The initial un-optimized structure of *sn*-2-LysoPC-DHA was constructed similar to a computational model based on an earlier study [14]. Following this initial model geometry, other structures were generated and subjected to geometry optimization.

We calculated the molecular electrostatic potential (ESP) maps and lipophilic potentials at the surfaces of molecules. EPS energy maps were generated by using Jmol program, a computer software for molecular modelling chemical structures in three-dimensions. These molecular properties can be derived from the 3-D structures and could be related to the functions of the molecules. The distribution of the hydrophobic potentials, characteristic of an amphipathic structure, can be calculated at the surface of Lyso-PC-DHA, Lyso-PE-DHA and Lyso-PS-DHA.

2.9. Statistical analysis

All experiments were conducted in triplicates. The obtained results were expressed as mean ± SD of three values and analyzed by using GraphPad Prism 9.3.1 software. The significance level was considered at *P* values of less than 0.05 based on *t*-test or analysis of variance (ANOVA), followed by Bonferroni test. Data were tested for normality applying Shapiro-Wilk test.

3. Results

3.1. LC-MS analysis of non-esterified DHA and produced LysoPL-DHA

As previously stated, DHA and produced LysoPL-DHA were quantified using LC-MS under optimized LC-ESI-MS conditions mentioned in Table 2.

For DHA, we proceeded with external calibration as shown in Fig. 3A and B. For quantification of produced LysoPL-DHA (Fig. 3C–E,

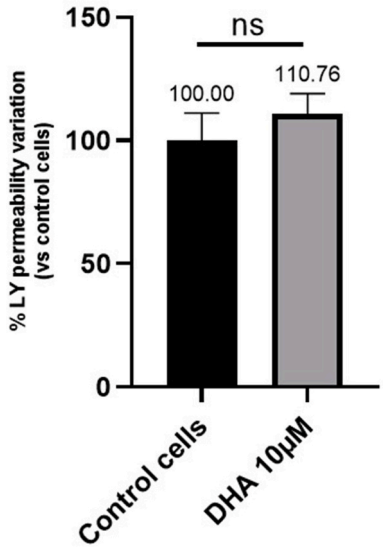

Fig. 4. BBB permeability to Lucifer yellow in the absence (Control cells) or in presence of DHA 10 µM in the luminal compartment of human BBB model during 180 min hBLECs

monolayer tightness was evaluated by the parallel assessment of the permeability of fluorescent marker, Lucifer yellow (LY). These experiments were conducted using Polyethylene terephthalate (PET) inserts.

Results represent the mean value ± SD (n = 3). Control permeability was 0.55 ± 0.06 x 10^{-3} cm min^{-1}. Statistical analysis was performed through GraphPad Prism 9.3.1 software using *t*-test.

G), sharp peaks were acquired. The same was observed for different LysoPL-18:1 standards.

The retention times of DHA, LysoPC-DHA, LysoPE-DHA, and LysoPS-DHA were respectively 6.22, 3.60, 5.17, and 5.10 min which are comparatively short as compared to previous normal phase liquid chromatography [43]. The peak area repeatability of five replicate analysis was less than 10 %. Linear responses were verified between peaks area and concentration in the broad ranges, therefore confirming that the process was pertinent for lipidomic elucidation.

Under MS optimized conditions, the product ion patterns of the different LysoPL, including LysoPC, LysoPE, and LysoPS, were dominated by the same collision-induced dissociation pathway, which simplifies understanding ESI-MS data. Compared to the positive ionization mode, more instructive data and higher signal-to-noise ratios could be observed in the negative ionization mode, allowing simultaneous ionization of PL within a single analytical run [44]. The product ions detected at 283 and 229 *m/z* values are considered characteristic fragments of DHA under the negative ionization mode [45]. While, the main typical LysoPC fragments in the positive ionization mode are the product ions detected at 184, 104, and 86 *m/z*. The product ion at 184 *m/z* is attributed to the phosphocholine group, and considered as an important parameter for LysoPC structure [46]. In the negative ionization mode, LysoPE pathway of $[M-H]^-$ was characterized by the abundant loss of 197 Da (neutral cyclic glycerophosphate ester) and the formation of carboxylate anions (R_1COO^-) from the fatty acyl groups [47]. In addition, the analysis of LysoPS precursor was performed under the negative ionization mode with LC-MS/MS monitoring for the neutral loss of 87 atomic mass units, signifying the loss of serine, a characteristic of phosphatidylserine species [47].

3.2. In vitro BBB tightness and toxicity of different DHA forms

In all experiments, the hBLECs monolayer tightness was evaluated by the parallel assessment of the permeability of fluorescent marker, Lucifer yellow (LY). These experiments were conducted using Polyethylene terephthalate (PET) inserts. Similar results for LY permeability were obtained in presence or absence of DHA at 10 μM as illustrated in Fig. 4. These results reveal the absence of toxicity of non-esterified DHA towards hBLECs of the human BBB model.

The similar results for LY permeability obtained in the presence or absence of the tested lipid compounds at different concentrations demonstrated the absence of toxicity of these molecules towards hBLECs of the human BBB model (Fig. 5). It should be noted a slight significant increase of LY permeability in the presence of LysoPC-DHA at 10 μM, which demonstrated a slight toxicity on the hBLEC monolayer.

3.3. Passage of non-esterified DHA and DHA esterified in lysophospholipids across hBLEC monolayer

We aimed to compare the passage of non-esterified DHA and three different forms of LysoPL-DHA (including LysoPC-DHA, LysoPE-DHA, LysoPS-DHA) across hBLECs in order to identify the privileged carrier of DHA to the brain. For the transport study, we conducted the experiments in triplicates with different concentrations (1 and 10 μM).

For all experiments, the recovery of lipids, after incubation with non-esterified DHA, LysoPC-DHA, LysoPE-DHA or LysoPS-DHA,

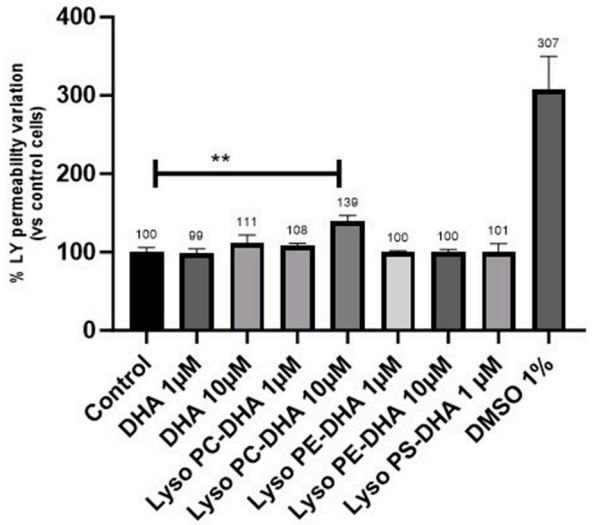

Fig. 5. BBB permeability to Lucifer yellow in absence (control cells) or in presence of DHA, LysoPC-DHA, LysoPE-DHA and LysoPS-DHA in luminal compartment of human BBB model during 180 min hBLECs
monolayer tightness was evaluated by the parallel assessment of the permeability of fluorescent marker, Lucifer yellow (LY). These experiments were conducted using Polyethylene terephthalate (PET) inserts.
Control permeability was $0.59 \pm 0.02 \times 10^{-3}$ cm min^{-1}. Results represent the mean value ± SD (n = 3). Statistical analysis was performed through GraphPad Prism 9.3.1 software using *t*-test.

was evaluated in different BBB compartments after LC-MS analysis as previously described.

First, we compared the cumulative time course of lipids recovered in the abluminal medium at 30 min, 60 min and 120 min after incubation with DHA, LysoPC-DHA, LysoPE-DHA or LysoPS-DHA (Fig. 6). At 30 min, 60 min and 120 min post-incubation, all tested LysoPL-DHA displayed a higher recovery in the abluminal medium in comparison to non-esterified DHA with significant differences (Fig. 6A, B, 6C). As illustrated in Fig. 6A, at 30 min, when comparing the percentage of passage per min, there was no significant difference between LysoPC-DHA, LysoPE-DHA and LysoPS-DHA with respectively 2.67 % ± 0.59, 2.92 % ± 0.05 and 2.25 % ± 0.32 whereas a significant difference with $p < 0{,}001$ was noticed when compared to DHA exhibiting 0.54 % ± 0.02. Moreover, at 60 min post-incubation, a significant difference between DHA and all other tested lipids was observed with $p < 0{,}01$ (Fig. 6B). Additionally, LysoPC-DHA, LysoPE-DHA and LysoPS-DHA were recovered respectively in the abluminal medium with 1.9 % ± 0.62, 2.07 % ± 0.05 and 2.25 % ± 0.32. These results were also relevant at 120 min post-incubation (Fig. 6C). DHA recovery (0.40 % ± 0.005) was significantly lower than LysoPC-DHA (1.32 % ± 0.21), LysoPE-DHA (1.39 % ± 0.04) and LysoPS-DHA (1.53 % ± 0.16) with $p < 0{,}001$ when compared to LysoPC-DHA, LysoPE-DHA and $p < 0{,}0001$ when compared to LysoPS-DHA (Fig. 6C).

Furthermore, we calculated the apparent coefficient permeability (Papp) of DHA, LysoPC-DHA, LysoPE-DHA, LysoPS-DHA, 180 min after transport across hBLECs (Fig. 7). Our results revealed that LysoPS-DHA revealed the highest apparent coefficient permeability with 85.87 x 10^{-6} cm s^{-1} ± 4.25 and was significantly different than DHA, LyoPC-DHA and LysoPE-DHA exhibiting respectively 26.04 x 10^{-6} cm s^{-1} ± 0.11, 63.71 x 10^{-6} cm s^{-1} ± 5.7 and 75.04 x 10^{-6} cm s^{-1} ± 1.99. Additionally, DHA revealed the lowest % of passage across the hBLECs when compared with to other Lyso-PL.

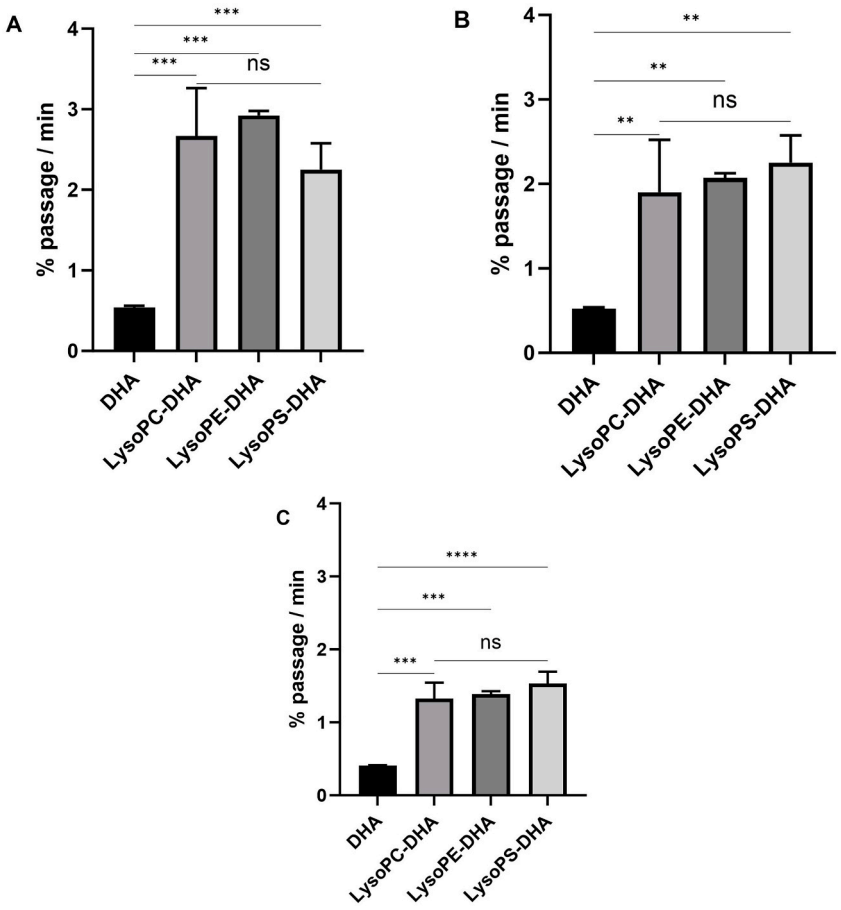

Fig. 6. Percentage of lipids recovered per min in abluminal medium, in presence of Human Brain Like Endothelial Cells (hBLECs), after incubation with 10 μM of DHA, LysoPC-DHA, LysoPE-DHA and LysoPS-DHA for 30 min (A), 60 min (B) and 120 min (C).
DHA and LysoPL-DHA were incubated at 10 μM on the luminal compartment of the human BBB model. DHA and LysoPL-DHA were added in 500 μL of RH buffer in the apical compartment of the insert of the BBB model. The insert is then placed on a 12-well plate filled with 1.5 mL of RH buffer. At 30, 60, 120 min, the inserts are placed in a new RH-filled well. At the end of the experiments, samples were taken from each compartment. Total lipids of abluminal medium were extracted according to the method of Bligh and Dyer [37]. The percentage of lipids recovered per min in abluminal medium was evaluated by dividing the quantity of lipids (DHA or LysoPL-DHA) that cross the BBB by the initial quantity added in the luminal compartment of the model and then divided by the time factor. Results are expressed as percentage of passage per min and presented as ±SD of three values. Groups were compared by analysis of variance (ANOVA) followed by Bonferroni test. ns: not significant; *: $p < 0{,}05$; **: $p < 0{,}01$; ***: $p < 0{,}001$; ****: $p < 0{,}0001$. Statistical analysis was performed through GraphPad Prism 9.3.1 software.

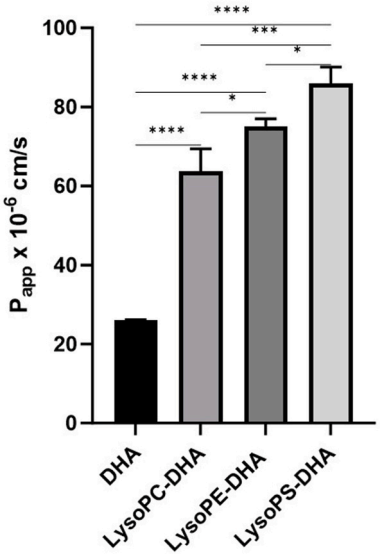

Fig. 7. Apparent coefficient permeability of DHA, LysoPC-DHA, LysoPE-DHA, LysoPS-DHA at 10 μM, 180 min after transport across hBLECSs. The endothelial apparent coefficient (Papp) of DHA and LysoPL-DHA were calculated as previously described by Santa-Maria AR et al., 2022 [39]. Papp, in cm.s^{-1} determinates the rate of appearance or flux (J, in amount.s^{-1}) of the compound in the receiver compartment, thereby, normalizing for membrane surface area (S, in cm^2) and initial donor concentration at t_0 (C_0, in amount.mL^{-1}). Results are presented as mean ± SD of three experiments. Groups were compared by analysis of variance (ANOVA) followed by Bonferroni test. ns: not significant; *: $p < 0,05$; **: $p < 0,01$; ***: $p < 0,001$; ****: $p < 0,0001$. Statistical analysis was performed through GraphPad Prism 9.3.1 software.

More interestingly, we studied the time course of apparent coefficient permeability of DHA, LysoPC-DHA and LysoPE-DHA at 30 min, 60 min, 120 and 180 min after transport across hBLECs (Fig. 8). Our results revealed that Papp decreases with the time especially for LysoPC-DHA and LysoPE-DHA but not for DHA. Since we maintained a gradient diffusion (with our 30, 30, 60 min transfers into a new plate), the observed decreases could be due to transporter saturation of LysoPL-DHA contrary to DHA that is transported *via* Mfsd2a [48,49].

Moreover, when compared to non-esterified DHA, significant differences were observed between tested LysoPL-DHA and DHA at 30 min ($p < 0,0001$), 60 min ($p < 0,0001$), 120 min ($p < 0,0001$), 180 min ($p < 0,01$) whereas no differences were noted between LysoPC-DHA and LysoPE-DHA.

Finally, we compared the intracellular accumulation of lipids in hBLECs 180 min after incubation with non-esterified DHA, LysoPC-DHA, LysoPE-DHA or LysoPS-DHA at 1 μM (Fig. 9).

Indeed, at 1 μM, DHA recovery in the endothelial cells was lower than the limit of detection and could not be detected through LC-

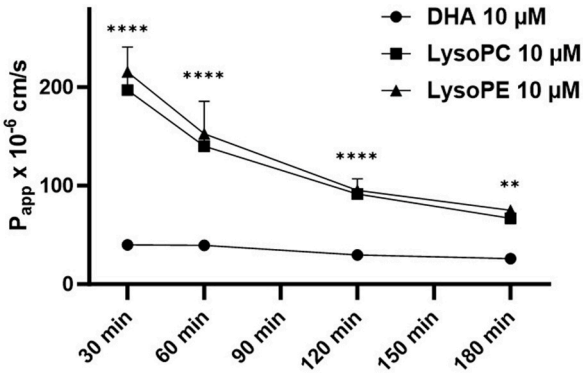

Fig. 8. Time course of apparent coefficient permeability of DHA, LysoPC-DHA and LysoPE-DHA, at 10 μM, during 180 min transport across hBLECs. The endothelial apparent coefficient (Papp) of DHA and LysoPL-DHA were calculated as previously described by Santa-Maria AR et al., 2022 [39]. Papp, in cm.s^{-1} determinates the rate of appearance or flux (J, in amount.s^{-1}) of the compound in the receiver compartment, thereby, normalizing for membrane surface area (S, in cm^2) and initial donor concentration at t_0 (C_0, in amount.mL^{-1}). Papp of DHA, LysoPC-DHA, LysoPE-DHA, LysoPS-DHA were determined at 30, 60, 120 and 180 min at 10 μM. Results are presented as mean ± SD of three experiments. Groups were compared by analysis of variance (ANOVA) followed by Bonferroni test. ns: not significant; *: $p < 0,05$; **: $p < 0,01$; ***: $p < 0,001$; ****: $p < 0,0001$. Statistical analysis was performed through GraphPad Prism 9.3.1 software.

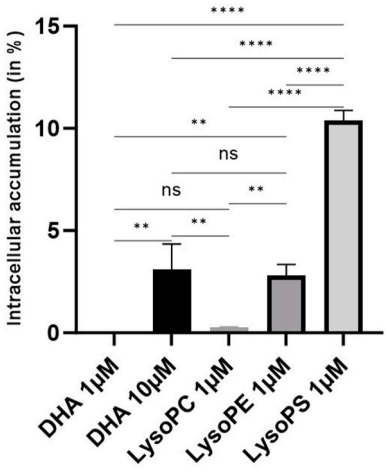

Fig. 9. Intracellular accumulation of non-esterified DHA and DHA esterified in LysoPL-DHA in hBLECs at 1 µM, 180 min after incubation. The same was calculated for DHA 10 µM.
DHA and LysoPL-DHA were incubated at 1 µM on the luminal compartment of the human BBB model. DHA and LysoPL-DHA were added in 500 µL of RH buffer in the apical compartment of the insert of the BBB model. The insert is then placed on a 12-well plate filled with 1.5 mL of RH buffer. At 30, 60, 120 min, the inserts are placed in a new RH-filled well. At the end of the experiments, samples were taken from each compartment. Total lipids of hBLECs were extracted according to Folch Method [38]. The percentage of intracellular accumulation in hBLECs was evaluated by dividing the quantity of lipids (DHA or LysoPL-DHA) that cross the BBB by the initial quantity added in the luminal compartment of the model. Results are expressed as percentage of passage per min and presented as ±SD of three values. Groups were compared by analysis of variance (ANOVA) followed by Bonferroni test. ns: not significant; *: $p < 0,05$; **: $p < 0,01$; ***: $p < 0,001$; ****: $p < 0,0001$. Statistical analysis was performed through GraphPad Prism 9.3.1 software.

MS analysis. The limit of detection and limit of quantification values of DHA were calculated according to the degree of freedom method by the analysis of 7 replicates of DHA at 0.05 µM as the lowest acceptable concentration that could be quantified in the calibration curve. Three ion transitions were detected for DHA (Table 1). The limit of quantification for DHA was set as the lowest concentration tested in which ion transitions had average accuracies between 80 and 120 % and precision ≤20 % relative standard deviation, based on at least 7 replicates. The blank sample obtained for validation did not contain any DHA at the levels being evaluated. Therefore, background subtraction was used to calculate accuracy of the fortification when determining the limit of quantification. The limit of quantification was determined to be 0.05 µM for ion transitions of DHA. The limit of detection was calculated by multiplying the standard deviation of the 7 replicates by the t-value (3.143) at 99 % confidence level (t0.99) at degree of freedom value of 6. The limit of detection was found to be 0.035 µM.

As illustrated in Fig. 9, DHA and LysoPC-DHA at 1 µM poorly accumulates within hBLECs, accumulation under the limit of quantification for DHA and 0.28 ± 0.02 % for LysoPC-DHA. On the other hand, LysoPS-DHA at 1 µM exhibited the higher recovery (10.39 ± 0.49 %) in hBLECs in comparison to all other tested lipids with significant differences ($p < 0,0001$). Additionally, when we calculated the intracellular accumulation of DHA at 10 µM, we noticed that, at high concentration, DHA accumulates at 3.11 ± 1.24 % very close to LysoPE-DHA intracellular accumulation which was 2.79 ± 0.55 % with no significant difference (Fig. 9).

3.4. Molecular modeling of lysophospholipids with DHA

Electrostatic potential maps (ESP maps) and optimized 3D structures of *sn-1* and *sn-2* LysoPL-DHA including LysoPC-DHA, LysoPE-DHA and LysoPS-DHA are shown respectively in upper and lower level of Fig. 10. More specifically, the optimized 3D structures of 1-docosahexaenoyl,2-lyso-glycerophosphatidylethanolamine (*sn-1*-LysoPE-DHA) and 1-docosahexaenoyl,2-lyso-glycerophosphatidyl-serine (*sn-1*-LysoPS-DHA) were represented in Fig. 10.

The first noticeable observations in ESP maps are that the charge distribution of *sn-1* and *sn-2* isomers had similar patterns. For all six lysophospholipids, hydrophobic regions characterized by green color in the maps were localized around docosahexaenoyl group with green color in ESP map. In docosahexaenoyl group, all the alkenes have cis conformations.

In *sn-1*-LysoPC-DHA and *sn-2*-LysoPC-DHA (Fig. 10A and B), quaternary ammonium group in choline moiety carried positive charge density which was indicated by blue color in the ESP map. Two of the phosphate oxygen atoms had negative charge density characterized with yellow orange color in ESP with respect to other atoms. Moreover, looking to their 3D structures, *sn-1*-LysoPC-DHA and *sn-2*-LysoPC-DHA isomers had different relative orientation of glycerophosphatidylcholine (GPC) with respect to docosahexaenoyl group. It can be also stated that choline groups had also different conformation for both isomers.

In *sn-1*-LysoPE-DHA and *sn-2*-LysoPE-DHA (Fig. 10C and D), ammonium group of ethanolamine, inferred from bright blue color in ESP, carried less positive charge density as compared to the quaternary ammonium group of choline in LysoPC-DHA. This indicated that instead of ammonium functionality, it resembled to amine functionality. Indeed, the optimized 3D structures of *sn-1*-LysoPE-DHA (Figs. 10A and 11A) in Fig. 11 showed that the nitrogen atom was very close to one of the O atoms of the phosphate group. One of the H

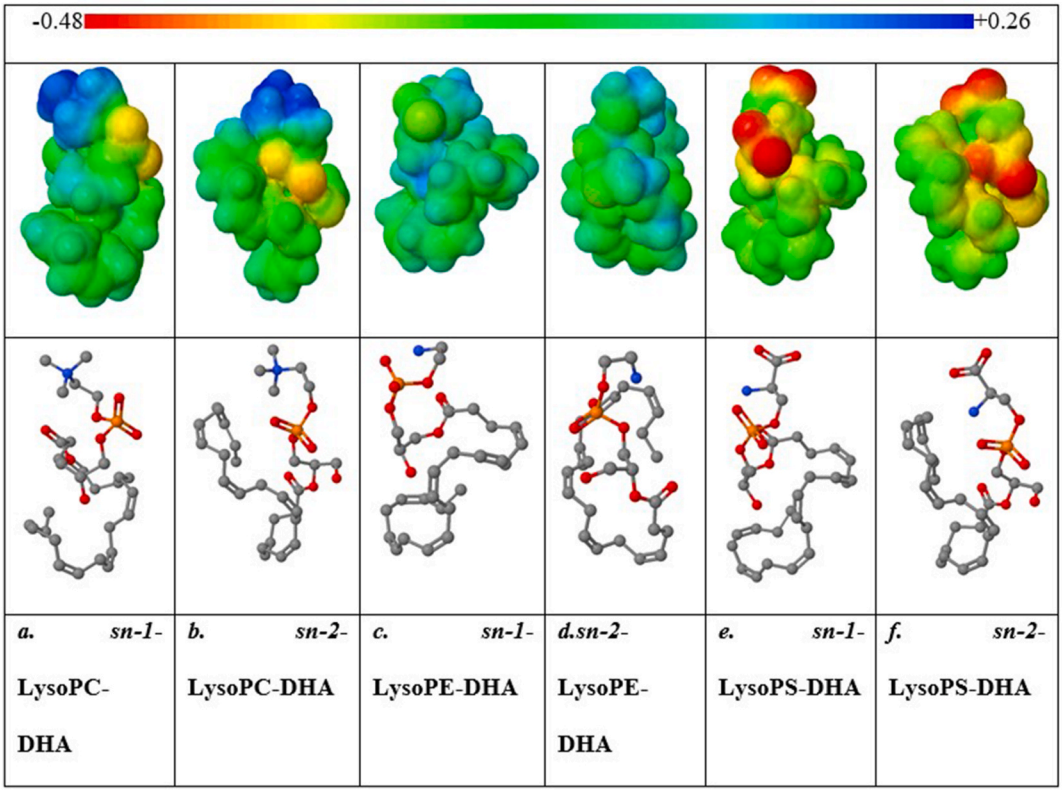

Fig. 10. Molecular electrostatic potential (ESP) maps and optimized 3D structures of LysoPL-DHA. All 3D chemical structures and maps were created using JMOL software.

After energy minimization and evaluation with Gaussian 09 software, one model of LysoPC-DHA, LysoPE-DHA and LysoPS-DHA was considered as representative of the 3-D structure of all LysoPL-DHA. Density functional theory (DFT) calculations was performed to optimize the geometries of the synthesized LysoPL-DHA by using M06-2X DFT functional with Gaussian 09 package. M06-2X functional was selected due to its better performance. Minimum energy geometries were validated with the frequency calculations requiring no imaginary eigenvalues. The initial un-optimized structure of *sn*-2-LysoPC-DHA was constructed similar to a computational model based on Hachem et al., 2016 [25]. Following this initial model geometry, other structures were generated and subjected to geometry optimization.The molecular electrostatic potential (ESP) maps and lipophilic potentials at the surfaces of molecules were generated by using Jmol program, a computer software for molecular modelling chemical structures in three-dimensions. The distribution of the hydrophobic potentials, characteristic of an amphipathic structure, were calculated at the surface of Lyso-PC-DHA, Lyso-PE-DHA and Lyso-PS-DHA.

For clarity reasons, all hydrogen atoms are hidden in the 3D structures.

a. 1-docosahexaenoyl,2-lyso-glycerophosphatidylcholine (*sn-1*-LysoPC-DHA);
b. 1-lyso,2-docosahexaenoyl-glycerophosphatidylcholine (*sn-2*-LysoPC-DHA);
c. 1-docosahexaenoyl,2-lyso-glycerophosphatidylethanolamine (*sn-1*-LysoPE-DHA);
d. 1-lyso,2-docosahexaenoyl-glycerophosphatidylethanolamine (*sn-2*-LysoPE-DHA);
e. 1-docosahexaenoyl,2-lyso-glycerophosphatidylserine (*sn-1*-LysoPS-DHA);
f. 1-lyso, 2-docosahexaenoyl- glycerophosphatidylserine (*sn-2*-LysoPS-DHA).

atoms at ammonium group was not anymore attached to N atom, instead it was attached to the O atom at the phosphate group. This clearly showed an intramolecular proton transfer process for the optimized 3D structure. Consequently, the ammonium group lost its positive charge density. In addition, the phosphate group lost its negative charge density.

As expected, ESP map for *sn-1*-LysoPE-DHA and *sn-2*-LysoPE-DHA did not show any negative charge density (represented by yellow orange color) at phosphate group. Alike GPC and docosahexaenoyl group in LysoPC-DHA isomers, glycerophosphatidylethanolamine (GPE) and docosahexaenoyl group had different relative orientations in both LysoPE-DHA isomers and GPE has different conformations for both isomers.

When studying ESP maps of *sn-1*-LysoPS-DHA and *sn-2*-LysoPS-DHA (Fig. 10E and F), negative charge densities around phosphate and carboxylate groups were observed. The ammonium groups of serines for both isomers did not carry any positive charge density implying that positive charge is somehow delocalized. The optimized 3D structure of *sn-1*-LysoPS-DHA (Fig. 11B) showed that three H-bonding interactions between serine and phosphate group delocalize the positive charge on the ammonium group as shown with black lines in Fig. 11B.

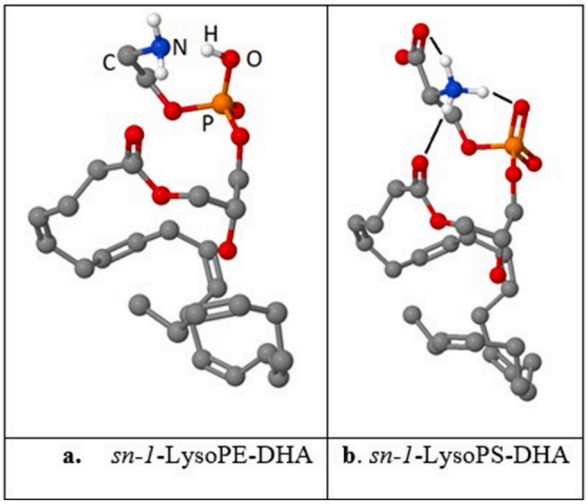

Fig. 11. Optimized 3D structures of 1-docosahexaenoyl,2-lyso-glycerophosphatidylethanolamine (*sn-1*-LysoPE-DHA); 1-docosahexaenoyl,2-lyso-glycerophosphatidylserine (*sn-1*-LysoPS-DHA)
After energy minimization and evaluation with Gaussian 09 software, one model of LysoPC-DHA, LysoPE-DHA and LysoPS-DHA was considered as representative of the 3-D structure of all LysoPL-DHA. Density functional theory (DFT) calculations was performed to optimize the geometries of the synthesized LysoPL-DHA by using M06-2X DFT functional with Gaussian 09 package. M06-2X functional was selected due to its better performance. Minimum energy geometries were validated with the frequency calculations requiring no imaginary eigenvalues. The initial un-optimized structure of *sn-1*-LysoPC-DHA was constructed similar to a computational model based on Hachem et al., 2016 [25]. Following this initial model geometry, other structures were generated and subjected to geometry optimization. The molecular electrostatic potential (ESP) maps and lipophilic potentials at the surfaces of molecules were generated by using Jmol program, a computer software for molecular modelling chemical structures in three-dimensions. The distribution of the hydrophobic potentials, characteristic of an amphipathic structure, were calculated at the surface of LysoPC-DHA, LysoPE-DHA and LysoPS-DHA. For clarity reasons, all hydrogen atoms except the ones that are shown with ivory color are hidden in the 3D structures. (For interpretation of the references to color in this figure legend, the reader is referred to the Web version of this article.)

4. Discussion

The cerebral bioavailability of DHA in comparison to LysoPC-DHA and other LysoPL-DHA forms including LysoPE-DHA, and LysoPS-DHA are not yet explored. Hence, in the present study, we investigated the passage of non-esterified DHA and DHA esterified in LysoPC, LysoPE and LysoPS through an *in vitro* model of human BBB in order to identify the privileged carrier of DHA to the brain.

We first synthesized LysoPC-DHA, LysoPE-DHA, and LysoPS-DHA *via* enzymatic hydrolysis of *sn-1* position respectively of PC-DHA, PE-DHA and PS-DHA as described previously since these lipids are not commercially available. To purify, quantify and characterize the produced molecules, we optimized a novel LC-MS approach including validation of MRM conditions and this approach can be integrated in lipidomic database since it is the first time to document such analysis. Following, we assessed the toxicity of DHA, LysoPC-DHA, LysoPE-DHA and LysoPS-DHA at different concentrations on a human model of Blood-Brain-Barrier that was developed at the Blood-Brain-Barrier Research Unit at Artois University under the supervision of Prof. Gosselet. For toxicity tests, Lucifer Yellow (LY, 25 μM) was used as a paracellular marker. Our results revealed the absence of toxicity of non-esterified DHA and all tested LysoPL-DHA towards hBLECs of the human BBB model at 1 and 10 μM.

Moreover, we investigated the endothelial apparent permeability and intracellular accumulation of non-esterified DHA, LysoPC-DHA, LysoPE-DHA and LysoPS-DHA.

When we compared the cumulative time course of lipids recovered in the abluminal medium at 30 min, 60 min and 120 min after incubation with DHA, LysoPC-DHA, LysoPE-DHA or LysoPS-DHA, all tested LysoPL-DHA displayed a higher recovery in the abluminal medium in comparison to non-esterified DHA with significant differences with $p < 0{,}001$ whereas no significant difference between LysoPC-DHA, LysoPE-DHA and LysoPS-DHA was noticed.

Furthermore, when calculating the apparent coefficient permeability Papp of DHA, LysoPC-DHA, LysoPE-DHA, LysoPS-DHA 180 min after transport across hBLECs, we observed a constant percentage of DHA passage around 0.5 % per minute that corresponds to an apparent coefficient permeability Papp of 26×10^{-6} cm s^{-1}. All the tested LysoPL-DHA showed a highest % of passage across the BBB and Papp when compared with DHA.

More interestingly, LysoPS-DHA displays the highest Papp with 85.87×10^{-6} cm $s^{-1} \pm 4.25$ and was significantly different than DHA, LyoPC-DHA and LysoPE-DHA exhibiting respectively 26.04×10^{-6} cm $s^{-1} \pm 0.11$, 63.71×10^{-6} cm $s^{-1} \pm 5.7$ and 75.04×10^{-6} cm $s^{-1} \pm 1.99$. Furthermore, LysoPS-DHA had the highest intracellular accumulation at 1 μM with the higher recovery (10.39 ± 0.49 %) in hBLECs when compared to all other tested lipids with significant differences ($p < 0{,}0001$).

Additionally, we studied the time course of apparent coefficient permeability of DHA, LysoPC-DHA and LysoPE-DHA at 10 μM at 30 min, 60 min, 120 and 180 min after transport across hBLECs. We noticed that Papp decreases with the time particularly for LysoPC-

DHA and LysoPE-DHA but not for DHA. This observation could be due to transporter saturation of LysoPL-DHA differing from DHA that could transported across the BBB through passive diffusion. All these results can be potentially explained by the Electrostatic potential maps (ESP maps) and optimized 3D structures of the LysoPL that we investigated by using M06-2X 13 DFT functional with Gaussian 09 package and Jmol program. For the first time, the obtained results indicated that the hydrophobic moieties were localized around DHA group characterized by a *cis* conformation of all alkene functions. Furthermore, glycerophospholipids moieties, glycerophosphatidylcholine, glycerophosphatidylethanolamine, glycerophosphatidylserine, and DHA group, had dissimilar orientations. Consequently, further research is required to investigate whether these differences in orientations could influence the transfer of these lipids to the brain through the BBB, their cerebral metabolism and functions. Regarding charges' distribution, in *sn-2*-LysoPC-DHA, positive and negative charges were distributed between ammonium and phosphate moieties; however, in *sn*-2-LysoPE-DHA, due to intramolecular proton transfer, no clear separation of charges was observed. In *sn*-2-LysoPS-DHA, positive charge on ammonium moiety was delocalized and negative charge density was localized at carboxylate and phosphate groups due to H-bonding interactions between serine and phosphate groups. The effect of these dissimilarities should be further examined through *in vitro* and *in vivo* studies.

In the context of earlier research conducted within the same thematic, it was documented that different forms of DHA either non-esterified or esterified in PL and LysoPL, exhibited several beneficial effects in the human brain, including anti-inflammatory effects [50] as well as improved brain-derived neurotrophic factors, improved memory, cognition, spatial learning, and could be preventive for depression and other age-related neurodegeneration [51–54]. In human plasma and red blood cells, LysoPC-DHA, most abundant LysoPL-DHA, is associated to albumin and lipoproteins [55]. After LysoPC-DHA, LysoPE-DHA is the second highest LysoPL [56]. In the brain, LysoPE-DHA had prospective biological functions, and was reported to be implicated in the stimulation of neurite's growth [16]. Another LysoPL of interest is LysoPS-DHA which is found in the brain, heart, lung, liver, kidney, and colon [57], as well as in the immune system organs [58]. The total amount of LysoPS in organs was reported to be in the range of 1–10 μg/g. In addition, a tremendously trivial level was found in the blood. Conversely, LysoPS is presented in greater levels in serum suggesting that it can be produced during blood coagulation [59].

When compared to earlier studies, our findings line up with the data previously obtained *in vitro* through bovine BBB models and *in vivo* in rodents, mainly when comparing the cerebral bioavailability of DHA and LysoPC-DHA whereas no data are documented for the comparison of the fours tested lipids in our study [18–25].

Indeed, Bernoud et al., 1999 demonstrated the privileged passage of LysoPC-DHA in comparison to DHA at 5 μM and incubation time of 240 min across a bovine *in vitro* model of BBB, consisting of brain capillary endothelial cells and astrocytes, with a % of initial radioactivity in abluminal medium of 15 % for LysoPC-DHA and 5 % for DHA [19]. Likewise, Hachem et al., 2016, investigated the passage of DHA in comparison to AceDoPC® (considered a stabilized form of the physiological LysoPC-DHA) and PC-DHA, through the same model of BBB tested by Bernoud et al., 1999. The team showed a privileged passage of AceDoPC® across the BBB in comparison to DHA and PC-DHA with a % of initial radioactivity in the abluminal medium of 7.5 % for AceDoPC, 4.5 % for DHA and 4 % for PC-DHA [25].

Bazinet et al. proposed that circulating LysoPC-DHA had a longer half-life and higher brain/body partition coefficient as compared to the non-esterified DHA, while non-esterified DHA exhibited a greater net rate of entry into the brain [60]. This suggestion reveals that more LysoPC-DHA would target the brain upon intravenous administration as compared to the non-esterified DHA. In addition, it was reported that diets supplemented with high LysoPC-DHA levels could enrich the brain DHA and enhance memory relevant behavior in mice expressed APOE4 [61]. In another study, the levels of brain DHA were reported to be increased by more than 2-fold in normal adult mice fed on either *sn*-1 or *sn*-2-LysoPC-DHA, whereas the treatment by using equal amounts of non-esterified DHA did not significantly increase the levels of brain DHA [62].

Additionally, LysoPC-DHA administered in maternal mice has been reported to significantly enrich DHA levels in the fetal brain than DHA-esterified monoacylglycerols form [63]. Moreover, it was reported that LysoPC-DHA chylomicron produced in the liver of maternal mice, was transported through the bloodstream to the fetal brain *via* umbilical cord and placenta [64–66]. Consequently, LysoPC was always considered as the most effective carrier to transport DHA to the brain.

Moreover, the most effective PL-esterified DHA on the accretion of fetal brain DHA was investigated by preparing PC-esterified DHA, LysoPC DHA, PS-esterified DHA, and LysoPS-DHA [67]. The four PL-esterified DHA forms were served to maternal mice for 4 days. LysoPS-DHA was the most effective LysoPL structure for the accretion of fetal brain DHA. This was considered due to that DHA being more easily incorporated into serum in the form of LysoPL, particularly LysoPS-DHA, by transferring through the small intestinal ECs monolayer. In addition, it was concluded that the most frequently DHA carriers used, specifically TAG-esterified DHA, *sn*-2-PC-esterified DHA or ethyl esters did not improve the brain DHA, since they are absorbed as TAG, which is not proficiently converted to LysoPC-DHA in the liver. It was shown that di-DHA PC was only half as efficient as LysoPC-DHA based on the content of DHA, supporting the theory that only DHA from the *sn*-1 position of PC is efficiently transported into the brain. Also, in contrast to PC-DHA, there was no difference between LysoPC-DHA *sn*-1 and *sn*-2 isomers in their ability to enhance the brain DHA [68].

As previously mentioned, two isomers, *sn*-1 and *sn*-2 of LysoPL-DHA are known in the literature depending on the position of DHA moiety. Indeed, DHA is stored in tissues at *sn*-2 position of LysoPL-DHA, *sn*-2 position considered as physiological forms in human body [69]. Moreover, DHA migrates easily from the *sn*-2 position of LysoPC to the *sn*-1 position, which is more stable [70].

Despite this, it is essential to investigate the properties and functions of both *sn*-1 and *sn*-2-LysoPL-DHA in order to elucidate any similarities or differences, which might affect their intake and metabolism in the brain and other body tissues.

Finally, the novelty of LysoPS-DHA's higher permeability and accumulation in the brain, in comparison to LysoPC-DHA, LysoPE-DHA and non-esterified DHA, would help pave the way for future research and clinical applications mainly in the prevention and treatment of neurodegenerative diseases. A key factor is to elucidate the mechanism of passage of LysoPS-DHA across the BBB. In previous studies, the transporter Mfsd2a was shown to be involved in the cerebral accretion of DHA in *sn*-1 and *sn*-2 forms [48,49,51].

Based on our results in term of ESP maps and 3D structures, considering the fact that Mfsd2a was able to transport *sn*-1 and *sn*-2-LysoPC-DHA, we wonder whether any similar transporter in the brain, which may carry isomers of LysoPS-DHA, exists. In addition to *in vitro* studies, *in vivo* and *ex-vivo* experiments should be performed to decipher crossing mechanism and uptake of LysoPS-DHA in the brain.

5. Conclusion

In the context of possible prevention and treatment of neurodegenerative diseases, researches on the beneficial effects and targeting the brain with LysoPL-DHA have been considerably developed. In the present study, we suggested that LysoPS-DHA exhibits higher permeability and accumulation in the brain when compared to non-esterified DHA, LysoPC-DHA and LysoPE-DHA. Nevertheless, the mechanisms of LysoPS-DHA's incorporation into the brain must be further explored in order to identify the specific protein transporter for improving cerebral level of DHA. We recommend further *in vivo* studies for cerebral accretion of LysoPC-DHA, LysoPE-DHA and LysoPS-DHA in comparison to non-esterified DHA to confirm our findings obtained in the *in vitro* study. Furthermore, clinical studies for testing LysoPS-DHA as a substitute in the prevention and treatment of neurodegenerative conditions are suggested. Finally, the characterization of LysoPS-DHA could be of great relevance to pharmaceutical applications in the context of neurodegenerative diseases.

Data availability statement

The authors confirm that the data supporting the findings of this study are available within the article.

Funding sources

This work was supported by three Internal Funding awarded to Mayssa Hachem including Faculty Start Up FSU8474000365, ESIG8474000472 and RIG8474000575 at Khalifa University of Sciences and Technology, UAE. Fabien Gosselet received further funding from the French State and Region Hauts-de-France as part of CPER 2021–2027 MOSOPS project.

CRediT authorship contribution statement

Mayssa Hachem: Writing – review & editing, Writing – original draft, Supervision, Project administration, Funding acquisition, Conceptualization. **Abdelmoneim H. Ali:** Visualization, Investigation, Formal analysis. **Ibrahim Yildiz:** Visualization, Resources. **Christophe Landry:** Methodology, Formal analysis, Conceptualization. **Fabien Gosselet:** Writing – review & editing, Validation, Methodology, Investigation, Formal analysis.

Declaration of competing interest

The authors declare that they have no known competing financial interests or personal relationships that could have appeared to influence the work reported in this paper.

Acknowledgments

The authors thankfully acknowledge the support of the faculty, staff, and colleagues at the Department of Chemistry at Khalifa University of Sciences and Technology, Abu Dhabi, United Arab Emirates. Also, the research team of Blood-Brain Barrier laboratory, Artois University, Lens, Franc.

References

[1] N. Pathak, et al., Neurodegenerative disorders of alzheimer, parkinsonism, amyotrophic lateral sclerosis and multiple sclerosis: an early diagnostic approach for precision treatment, Metab. Brain Dis. (2021) 1–38.
[2] R.N. Lamptey, et al., A review of the common neurodegenerative disorders: current therapeutic approaches and the potential role of nanotherapeutics, Int. J. Mol. Sci. 23 (3) (2022) 1851.
[3] M. Hachem, et al., Brain targeting with docosahexaenoic acid as a prospective therapy for neurodegenerative diseases and its passage across blood brain barrier, Biochimie 170 (2020) 203–211.
[4] R.D. Semba, Perspective: the potential role of circulating lysophosphatidylcholine in neuroprotection against alzheimer disease, Adv. Nutr. 11 (4) (2020) 760–772.
[5] A. Lo Van, et al., Omega-3 docosahexaenoic acid is a mediator of fate-decision of adult neural stem cells, Int. J. Mol. Sci. 20 (17) (2019).
[6] S.C. Cunnane, et al., Fish, docosahexaenoic acid and Alzheimer's disease, Prog. Lipid Res. 48 (5) (2009) 239–256.
[7] M.A. Mori, et al., Neuroprotective effect of omega-3 polyunsaturated fatty acids in the 6-OHDA model of Parkinson's disease is mediated by a reduction of inducible nitric oxide synthase, Nutr. Neurosci. 21 (5) (2018) 341–351.
[8] M. Xiao, et al., DHA ameliorates cognitive ability, reduces amyloid deposition, and nerve fiber production in Alzheimer's disease, Front. Nutr. 9 (2022).
[9] W.C. Breckenridge, G. Gombos, I.G. Morgan, The lipid composition of adult rat brain synaptosomal plasma membranes, Biochim. Biophys. Acta 266 (3) (1972) 695–707.
[10] W.J. Lukiw, N.G. Bazan, Docosahexaenoic acid and the aging brain, J. Nutr. 138 (12) (2008) 2510–2514.
[11] F. Gao, et al., Whole-body synthesis-secretion rates of long-chain n-3 PUFAs from circulating unesterified alpha-linolenic acid in unanesthetized rats, J. Lipid Res. 50 (4) (2009) 749–758.

[12] A.J. Sinclair, Incorporation of radioactive polyunsaturated fatty acids into liver and brain of developing rat, Lipids 10 (3) (1975) 175–184.
[13] M. Belkouch, et al., The pleiotropic effects of omega-3 docosahexaenoic acid on the hallmarks of Alzheimer's disease, J. Nutr. Biochem. 38 (2016) 1–11.
[14] A. Lo Van, et al., Mechanisms of DHA transport to the brain and potential therapy to neurodegenerative diseases, Biochimie 130 (2016) 163–167.
[15] M. Hachem, et al., Docosahexaenoic acid (DHA) bioavailability in humans after oral intake of DHA-containing triacylglycerol or the structured phospholipid AceDoPC(®), Nutrients 12 (1) (2020).
[16] M. Hachem, H. Nacir, Emerging role of phospholipids and lysophospholipids for improving brain docosahexaenoic acid as potential preventive and therapeutic strategies for neurological diseases, Int. J. Mol. Sci. 23 (7) (2022).
[17] A. Lo Van, N. Bernoud-Hubac, M. Lagarde, Esterification of docosahexaenoic acid enhances its transport to the brain and its potential therapeutic use in brain diseases, Nutrients 14 (21) (2022).
[18] F. Thies, et al., Preferential incorporation of sn-2 lysoPC DHA over unesterified DHA in the young rat brain, Am. J. Physiol. 267 (5 Pt 2) (1994) R1273–R1279.
[19] N. Bernoud, et al., Preferential transfer of 2-docosahexaenoyl-1-lysophosphatidylcholine through an in vitro blood-brain barrier over unesterified docosahexaenoic acid, J. Neurochem. 72 (1) (1999) 338–345.
[20] M.K. Ahmmed, et al., Marine fish-derived lysophosphatidylcholine: properties, extraction, quantification, and brain health application, Molecules 28 (7) (2023) 3088.
[21] F. Thiés, et al., Unsaturated fatty acids esterified in 2-acyl-l-lysophosphatidylcholine bound to albumin are more efficiently taken up by the young rat brain than the unesterified form, J. Neurochem. 59 (3) (1992) 1110–1116.
[22] N. Bernoud-Hubac, et al., Specific uptake of DHA by the brain from a structured phospholipid, AceDoPC®, OCL 24 (2) (2017) D205.
[23] M. Lagarde, et al., AceDoPC, a structured phospholipid to target the brain with docosahexaenoic acid, OCL 23 (1) (2016) D102.
[24] M. Lagarde, et al., Biological properties of a DHA-containing structured phospholipid (AceDoPC) to target the brain, Prostagl. Leukot. Essent. Fat. Acids 92 (2015) 63–65.
[25] M. Hachem, et al., Efficient docosahexaenoic acid uptake by the brain from a structured phospholipid, Mol. Neurobiol. 53 (5) (2016) 3205–3215.
[26] S.T. Tan, et al., Emerging roles of lysophospholipids in health and disease, Prog. Lipid Res. 80 (2020) 101068.
[27] R. Shawahna, X. Decleves, J.M. Scherrmann, Hurdles with using in vitro models to predict human blood-brain barrier drug permeability: a special focus on transporters and metabolizing enzymes, Curr Drug Metab 14 (1) (2013) 120–136.
[28] M.P. Dehouck, et al., Quantitative targeted absolute proteomics for better characterization of an in vitro human blood-brain barrier model derived from hematopoietic stem cells, Cells 11 (24) (2022).
[29] E. Melander, et al., Differential blood-brain barrier transport and cell uptake of cyclic peptides in vivo and in vitro, Pharmaceutics 15 (5) (2023).
[30] E. Di Biase, et al., GM1 oligosaccharide crosses the human blood-brain barrier in vitro by a paracellular route, Int. J. Mol. Sci. 21 (8) (2020).
[31] M. Devos, et al., Enzymatic hydrolysis of phospholipids from Isochrysis galbana for docosahexaenoic acid enrichment, Enzym. Microb. Technol. 39 (4) (2006) 548–554.
[32] F. Shimizu, et al., Peripheral nerve pericytes modify the blood-nerve barrier function and tight junctional molecules through the secretion of various soluble factors, J. Cell. Physiol. 226 (1) (2011) 255–266.
[33] D.C. Pedroso, et al., Improved survival, vascular differentiation and wound healing potential of stem cells co-cultured with endothelial cells, PLoS One 6 (1) (2011) e16114.
[34] R. Cecchelli, et al., A stable and reproducible human blood-brain barrier model derived from hematopoietic stem cells, PLoS One 9 (6) (2014) e99733.
[35] M.C. Lucana, et al., BrainBike peptidomimetic enables efficient transport of proteins across brain endothelium, RSC Chem Biol 5 (1) (2024) 7–11.
[36] R. Cecchelli, et al., In vitro model for evaluating drug transport across the blood-brain barrier, Adv. Drug Deliv. Rev. 36 (2–3) (1999) 165–178.
[37] E.G. Bligh, W.J. Dyer, A rapid method of total lipid extraction and purification, Can. J. Biochem. Physiol. 37 (8) (1959) 911–917.
[38] J. Folch, M. Lees, G.H. Sloane Stanley, A simple method for the isolation and purification of total lipids from animal tissues, J. Biol. Chem. 226 (1) (1957) 497–509.
[39] A.R. Santa-Maria, et al., Transport studies using blood-brain barrier in vitro models: a critical review and guidelines, Handb. Exp. Pharmacol. 273 (2022) 187–204.
[40] Y. Zhao, D. Truhlar, The M06 suite of density functionals for main group thermochemistry, thermochemical kinetics, noncovalent interactions, excited states, and transition elements: two new functionals and systematic testing of four M06-class functionals and 12 other functionals, Theor. Chem. Acc. 120 (1–3) (2008) 215–241.
[41] Frisch, M.J., et al., *Gaussian 09*. 2009, Gaussian, Inc.: Wallingford, CT, USA.
[42] Y. Zhao, D.G. Truhlar, Applications and validations of the Minnesota density functionals, Chem. Phys. Lett. 502 (1–3) (2011) 1–13.
[43] G. Shui, et al., Characterization of substrate preference for Slc1p and Cst26p in Saccharomyces cerevisiae using lipidomic approaches and an LPAAT activity assay, PLoS One 5 (8) (2010) e11956.
[44] J. Xue, et al., Comprehensive screening for EPA/DHA-Structured phospholipids in aquatic products by a specific precursor ion scanning-based HILIC-MS/MS method, J. Agric. Food Chem. (2023).
[45] R. Doyle, LC-MS/MS Quantitative Analysis of Polyunsaturated Omega 3, 6,7 and 9 Fatty Acids in Serum for Research Use, 2017.
[46] B. Brügger, et al., Quantitative analysis of biological membrane lipids at the low picomole level by nano-electrospray ionization tandem mass spectrometry, Proc. Natl. Acad. Sci. USA 94 (6) (1997) 2339–2344.
[47] N. Fang, S. Yu, T.M. Badger, LC-MS/MS analysis of lysophospholipids associated with soy protein isolate, J. Agric. Food Chem. 51 (23) (2003) 6676–6682.
[48] D.Q. Quek, et al., Structural insights into the transport mechanism of the human sodium-dependent lysophosphatidylcholine transporter MFSD2A, J. Biol. Chem. 291 (18) (2016) 9383–9394.
[49] L.N. Nguyen, et al., Mfsd2a is a transporter for the essential omega-3 fatty acid docosahexaenoic acid, Nature 509 (7501) (2014) 503–506.
[50] M. Hachem, SARS-CoV-2 journey to the brain with a focus on potential role of docosahexaenoic acid bioactive lipid mediators, Biochimie 184 (2021) 95–103.
[51] D. Sugasini, et al., Enrichment of brain docosahexaenoic acid (DHA) is highly dependent upon the molecular carrier of dietary DHA: lysophosphatidylcholine is more efficient than either phosphatidylcholine or triacylglycerol, J. Nutr. Biochem. 74 (2019) 108231.
[52] P.C.R. Yalagala, et al., Dietary lysophosphatidylcholine-EPA enriches both EPA and DHA in the brain: potential treatment for depression, J. Lipid Res. 60 (3) (2019) 566–578.
[53] S.B. Scheinman, et al., LPC-DHA/EPA-Enriched diets increase brain DHA and modulate behavior in mice that express human APOE4, Front. Neurosci. 15 (2021) 690410.
[54] H.-Y. Kim, B.X. Huang, A.A. Spector, Molecular and signaling mechanisms for docosahexaenoic acid-derived neurodevelopment and neuroprotection, Int. J. Mol. Sci. 23 (9) (2022) 4635.
[55] D. Sugasini, et al., Dietary docosahexaenoic acid (DHA) as lysophosphatidylcholine, but not as free acid, enriches brain DHA and improves memory in adult mice, Sci. Rep. 7 (1) (2017) 11263.
[56] O. Quehenberger, et al., Lipidomics reveals a remarkable diversity of lipids in human plasma, J. Lipid Res. 51 (11) (2010) 3299–3305.
[57] Y. Zhao, S. Hasse, S.G. Bourgoin, Phosphatidylserine-specific phospholipase A1: a friend or the devil in disguise, Prog. Lipid Res. 83 (2021) 101112.
[58] S. Yaginuma, et al., Emerging roles of lysophosphatidylserine as an immune modulator, Immunol. Rev. (2023).
[59] J.E. Konkel, et al., Transforming growth factor-β signaling in regulatory T cells controls T helper-17 cells and tissue-specific immune responses, Immunity 46 (4) (2017) 660–674.
[60] R.P. Bazinet, N. Bernoud-Hubac, M. Lagarde, How the plasma lysophospholipid and unesterified fatty acid pools supply the brain with docosahexaenoic acid, Prostagl. Leukot. Essent. Fat. Acids 142 (2019) 1–3.
[61] S.B. Scheinman, et al., LPC-DHA/EPA-enriched diets increase brain DHA and modulate behavior in mice that express human APOE4, Front. Neurosci. 15 (2021) 690410.

[62] D. Sugasini, et al., Dietary docosahexaenoic acid (DHA) as lysophosphatidylcholine, but not as free acid, enriches brain DHA and improves memory in adult mice, Sci. Rep. 7 (1) (2017) 11263.
[63] A. Valenzuela, et al., Supplementing female rats with DHA-lysophosphatidylcholine increases docosahexaenoic acid and acetylcholine contents in the brain and improves the memory and learning capabilities of the pups, Grasas y aceites 61 (1) (2010) 16–23.
[64] D. Kritchevsky, Fatty acids, triglyceride structure, and lipid metabolism, J. Nutr. Biochem. 6 (4) (1995) 172–178.
[65] F. Thies, et al., Unsaturated fatty acids esterified in 2-acyl-1-lysophosphatidylcholine bound to albumin are more efficiently taken up by the young rat brain than the unesterified form, J. Neurochem. 59 (3) (1992) 1110–1116.
[66] H. Suzuki, et al., *Rapid incorporation of docosahexaenoic acid from dietary sources into brain microsomal, synaptosomal and mitochondrial membranes in adult mice.* International Journal for Vitamin and Nutrition research. Internationale Zeitschrift fur Vitamin-und Ernahrungsforschung, J. Int. Vitaminol. Nutr. 67 (4) (1997) 272–278.
[67] T. Tsushima, et al., Lysophosphatidylserine form DHA maybe the most effective as substrate for brain DHA accretion, Biocatal. Agric. Biotechnol. 3 (4) (2014) 303–309.
[68] D. Sugasini, et al., Enrichment of brain docosahexaenoic acid (DHA) is highly dependent upon the molecular carrier of dietary DHA: lysophosphatidylcholine is more efficient than either phosphatidylcholine or triacylglycerol, The Journal of nutritional biochemistry 74 (2019) 108231.
[69] M. Picq, et al., DHA metabolism: targeting the brain and lipoxygenation, Mol. Neurobiol. 42 (1) (2010) 48–51.
[70] M. Croset, et al., Characterization of plasma unsaturated lysophosphatidylcholines in human and rat, Biochem. J. 345 (Pt 1) (2000) 61–67. Pt 1.